Computing Vessel Velocity from Single Perspective Projection Images

Jose Luis Huillca* and Leandro A. F. Fernandes
Instituto de Computação
Universidade Federal Fluminense (UFF),
Av. Gal. Milton Tavares de Souza, s/n, 24210-346, Niterói, RJ, Brazil

***Abstract*—The Master's Thesis presented an image-based approach to estimate the speed of moving vessels from their traces on the water surface. Vessels moving at constant heading and speed display a familiar V-shaped pattern which only differs from one to another by the wavelength of their transverse and divergent components. Such wavelength is related to vessel speed. We use planar homography and natural constraints on the geometry of ships' wake troughs to compute vessel speed from single optical images acquired by conventional cameras. Experiments show that our approach produces compelling results, which are in accordance with true data available for the observed vessels.**

I. Introduction

One of the most important technological advances in the maritime industry is electronic navigation [1]. These systems keep the pilot informed of the location and speed of nearby vessel's, as long as they are under system monitoring. Unfortunately, many vessels are not equipped with such systems. As a result, visual contact still plays an important role in decision making, especially at close range.

The importance of visual contact must be taken into account while commercial, military, and recreational navigation move toward the self-sailing ships era. The problem is that radars and other sensors may fail to detect stealth ships and non-metallic targets, because they reflect a very low amount of radiation. As a result, computer vision techniques for estimating ships' relative location and speed from visual clues will probably be an important component of self-sailing systems.

In Jose's Master's Thesis, we present a method for computing the speed of vessels directly from single perspective projection images acquired by conventional cameras (Fig. 1). Our approach is based on projective geometry and estimates the ship speed using the structure of Kelvin waves [2]. Our key observation is that navigating vessels (even stealth ones) leave traces of their motion in the form of wake patterns on the water surface. In 1887, Lord Kelvin demonstrated how to model those features as a function of speed [2].

The advantages of the proposed approach are twofold. First, the use of single images allows the estimation of the speed of nearby vessels from each frame of a video sequence independently. Estimate speed from motion in video sequences, on the other hand, would be a challenging task due to the natural movement of both reference and target ships as a result of wave action. Second, ship wakes are more distinct than the hulls and can be observed in optical images.

The *main contribution* of this work is a technique for computing vessel speed as an inverse Kelvin wake problem using data extracted from single optical images. We have performed experiments on images of different moving vessels. Results comparing the velocities estimated by our approach with truth data from passenger vessels on a service route across the Guanabara Bay show the accuracy of our technique.

II. Related work

Vessel detection and tracking using computer vision-based systems are convenient solutions for measuring vessel speed [3]. A large number of algorithms estimate the vessel speed by analyzing the traces left by the vessel using Synthetic-Aperture Radar (SAR) imagery. For example, Panico et al. [4] contributed in the task of recovering the vessel speed through wake analysis. They developed a method for estimating calm sea speed and applied it to seven X-band SAR images. In their work, they exploit the well-known relationship between the wavelength that make up the Kelvin pattern and the vessel speed.

Other techniques estimate speed using image sequences taken with a digital camera. Broggi et al. [5] describes a method of detecting, measuring speed, and extracting statistics for vessels moving over a wide water surface using images stream taken from a gray–scale camera. They demonstrated stable vessel detection even with sea waves and strong light reflections. The speed was estimated by the $pixel/frame$ measurement, while our method estimates speed in real-world units like knots and meters per second *using a single image*.

SAR-based methods use data collected by airborne sensors, while the video-based techniques require fixed cameras to estimate speed from relative motion. The proposed approach does not have those issues because it uses a single image that could be taken by a lighthouse, a vessel or a drone.

III. Computing vessel speed

We assume that the camera was mounted at a given height h above sea level, in such a way that the target ship and the traces left by it can be observed (Fig. 1). The orientation of the camera in world space is estimated during the process. For each image acquired, the processing steps include: (i) estimate the vanishing line of the mean water plane; (ii) define the

*M.Sc. dissertation

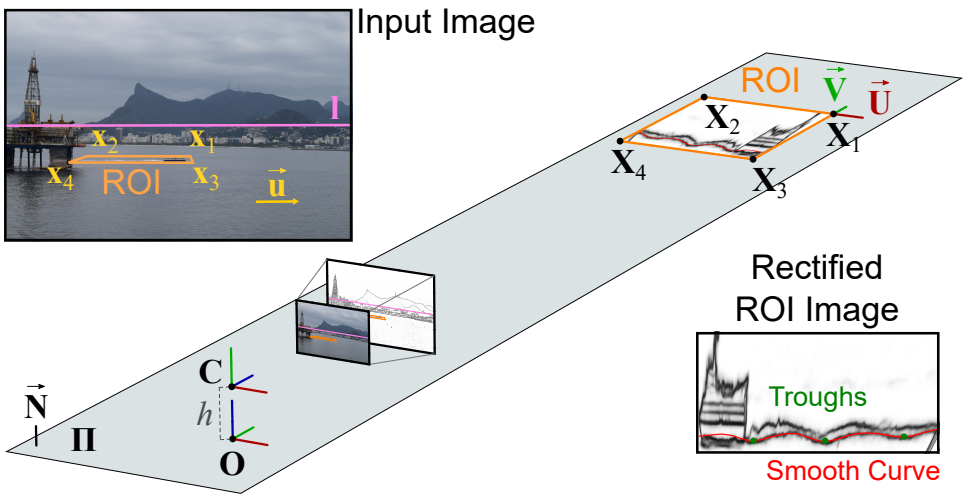

Fig. 1. We find the vanishing line $\mathbf{l}$ of the mean water plane $\mathbf{\Pi}$ using the input color image. From $\mathbf{l}$, camera height h, point $\mathbf{x}_1$ and vessel direction $\vec{\mathbf{u}}$ in image space, we estimate the vessel direction $\vec{\mathbf{U}}$ and corners $\mathbf{X}_i$ of the Region of Interest (ROI) in world space, and their projections $\mathbf{x}_i$. We use the edge image of the ROI in image space to find the wave arms of the traces left by the vessel. In the rectified ROI, we compute the wavelength and vessel speed from the Euclidean distance of the troughs of the smooth curve that approximates the wave arm closest to the camera centre $\mathbf{C}$. We intentionally flip the rectified ROI image to make the vessel go to the left.

corners of the Region of Interest (ROI) including the ship wake; (iii) find the wave arms and troughs present in the ROI; and (iv) estimate the vessel speed using the wavelength.

A. Vanishing line estimation

We use the Horizon Line in the Wild (HLW) algorithm [6] to detect the vanishing line of the water body automatically. The HLW algorithm estimates the left and right endpoints of the vanishing line of the most prominent plane observed in the input color image $\mathcal{I}$. In our equations, we represented the endpoints by homogeneous coordinates as vectors $\mathbf{p}_l = (0, y_{\mathbf{p}_l}, 1)^T$ and $\mathbf{p}_r = (W-1, y_{\mathbf{p}_r}, 1)^T$, where W is the width of $\mathcal{I}$ and $y_{\mathbf{p}_l}$ and $y_{\mathbf{p}_r}$ are the vertical coordinates of the points returned by HLW. The vector $\mathbf{l} = (A, B, C)^T$ encoding the vanishing line of the mean water plane in homogeneous coordinates can be computed as the cross product of vectors $\mathbf{p}_l$ and $\mathbf{p}_r$ [7].

B. Definition of the corners of the ROI

The ROI must include the ship wake. It is defined in the input image $\mathcal{I}$ as the quadrilateral resulting from the projection of a rectangular region on the water surface (see Fig. 1). We find the set of corners $\{\mathbf{x}_k\}_{k=1}^4$ of the ROI in $\mathcal{I}$ from the reference corner $\mathbf{x}_1 = (x_{\mathbf{x}_1}, y_{\mathbf{x}_1}, 1)^T$, the direction $\vec{\mathbf{u}} = (x_{\vec{\mathbf{u}}}, y_{\vec{\mathbf{u}}}, 0)^T$ of the vessel in this image, the vanishing line $\mathbf{l}$, the camera calibration matrix $\mathbf{K}$, the ROI size $W_{ROI} \times H_{ROI}$ (in meters) in 3D-space, and the camera height h above sea level. We manually choose $\mathbf{x}_1$ and $\vec{\mathbf{u}}$ in image space in our experiments. However, automatic object detection techniques could be used in practical aplication of our technique. In this work, we extracted metadata from the image files to compute $\mathbf{K}$. W_{ROI} and H_{ROI} are constant values defined by the user.

The camera height h (in meters) is given by construction and is defined in meters as the distance between the camera and the mean water plane. We assume that the origin $\mathbf{O}$ of the world coordinate system (see Fig. 1) lies on the orthogonal projection of the camera centre $\mathbf{C}$ to the mean water plane $\mathbf{\Pi}$, the X and Y axes span $\mathbf{\Pi}$ and the Z-axis is parallel to the vector $\vec{\mathbf{N}}$ normal to $\mathbf{\Pi}$. We set $\mathbf{C} = (0, 0, h, 1)^T$ and compute its orientation with respect to the world's frame from the vanishing line $\mathbf{l}$. If the camera is mounted on a vessel's mast, its height h can be calculated from of the mast's height and its relative orientation to the normal vector $\vec{\mathbf{N}}$ (computed from the vanishing line). For drones, the vehicle needs to be able to determine its altitude. In our experiments, the camera was mounted on a tripod in a building. In this case, the camera height above the sea level is calculated as the sum of the heights h_g, h_f, h_t, and h_s representing, respectively, the ground height, the floor height, the tripod height, and the tide height $h = h_g + \delta h_f + h_t - h_s$, where δ is the floor number where the camera was mounted.

1) Finding the set of corners of the ROI: Let $\{\mathbf{X}_k\}_{k=1}^4$ be the set of corners of the ROI lying on plane $\mathbf{\Pi}$. The corner $\mathbf{X}_1 = (X_{\mathbf{X}_1}, Y_{\mathbf{X}_1}, 0, 1)^T$ is computed by tracing a ray from the camera to $\mathbf{\Pi}$ through point $\mathbf{x}_1$:

$$\mathbf{X}_1 = \left(-hX_{\vec{\mathbf{D}}}/Z_{\vec{\mathbf{D}}}, -hY_{\vec{\mathbf{D}}}/Z_{\vec{\mathbf{D}}}, 0, 1\right)^T, \tag{1}$$

where $\vec{\mathbf{D}} = (X_{\vec{\mathbf{D}}}, Y_{\vec{\mathbf{D}}}, Z_{\vec{\mathbf{D}}})^T = \mathbf{M}^{-1}\mathbf{x}_1$ is the direction of the traced ray, $\mathbf{M} = \mathbf{KR}$, and $\mathbf{R}$ is a rotation matrix whose columns correspond to the X, Y, and Z axes of the camera in world frame of reference (respectively, the red, green, and blue segments leaving $\mathbf{C}$ in Fig. 1). The columns of $\mathbf{R}$ are $\vec{\mathbf{R}}_1 = \vec{\mathbf{R}}_3 \times \vec{\mathbf{R}}_2$, $\vec{\mathbf{R}}_2 = \text{unit}((1,0,0)^T \times \vec{\mathbf{R}}_3)$, and $\vec{\mathbf{R}}_3 = \text{unit}(\text{up}(\mathbf{K}^T\mathbf{l}))$. The unit function normalizes the vector to have unit length and the up function changes the orientation of $\vec{\mathbf{R}}_3$ if its $Y_{\vec{\mathbf{R}}_3}$ coordinate is negative. That operation is necessary to correct the hand of the camera coordinate system by forcing the $\vec{\mathbf{R}}_2$ vector to point upward,

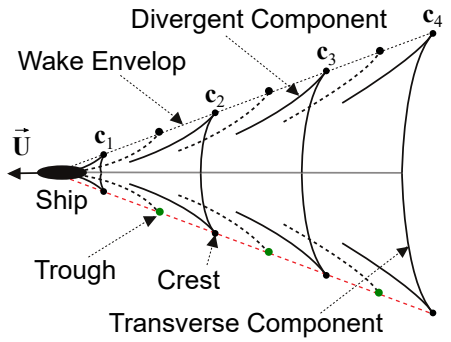

Fig. 2. The Kelvin wake structure, indicating the transverse and divergent components, and the crests and troughs of the wave arms.

like the normal vector $\vec{\mathbf{N}}$ of the mean water plane and the Z-axis of the world frame of reference (see Fig 1), while $\vec{\mathbf{R}}_1$ and $\vec{\mathbf{R}}_3$ point to the right and front, respectively.

$\mathbf{X}_2$, $\mathbf{X}_3$, and $\mathbf{X}_4$ are computed by translating $\mathbf{X}_1$ by W_{ROI} and H_{ROI} in directions $\vec{\mathbf{U}} = \text{unit}(\mathbf{A}\vec{\mathbf{E}})$ and $\vec{\mathbf{V}} = \mathbf{B}\vec{\mathbf{U}}$ on plane $\mathbf{\Pi}$:

$$\mathbf{X}_2 = \mathbf{X}_1 - W_{ROI}\vec{\mathbf{U}}, \tag{2a}$$

$$\mathbf{X}_3 = \mathbf{X}_1 - H_{ROI}\vec{\mathbf{V}}, \tag{2b}$$

$$\mathbf{X}_4 = \mathbf{X}_1 - W_{ROI}\vec{\mathbf{U}} - H_{ROI}\vec{\mathbf{V}}, \tag{2c}$$

where $\vec{\mathbf{U}}$ is the direction of the vessel in world coordinates, and $\vec{\mathbf{V}}$ is a perpendicular direction computed by rotating $\vec{\mathbf{U}}$ in $\mathbf{\Pi}$ through an angle of $\pi/2$. Thus, $\mathbf{B}$ is a constant rotation matrix. Here, $\vec{\mathbf{E}} = (X_{\vec{\mathbf{E}}}, Y_{\vec{\mathbf{E}}}, Z_{\vec{\mathbf{E}}})^T = \mathbf{M}^{-1}\vec{\mathbf{u}}$ is the back-projection of $\vec{\mathbf{u}}$ (an improper point) to world coordinates, and $\mathbf{A}$ encodes the orthogonal projection on $\mathbf{\Pi}$.

Finally, the corners of the ROI in $\mathcal{I}$ are computed as:

$$\mathbf{x}_k = \mathbf{P}\mathbf{X}_k, \tag{3}$$

where $k \in \{2, 3, 4\}$, $\mathbf{P} = \mathbf{M}\left(\mathbf{I} \mid -\tilde{C}\right)$ is the 3×4 camera matrix, $\mathbf{I}$ is a 3×3 identity matrix, and $\tilde{C} = (0, 0, h)^T$.

C. Finding the wave arms and troughs

We use the edge image $\mathcal{B}$ of the color image $\mathcal{I}$ to find the wave arms. The Richer Convolutional Features algorithm [8] was used to compute the edge image. To avoid processing the whole image or working with a non-rectangular ROI, the procedure for finding the wave arms considers a small portion of $\mathcal{B}$ defined as the axis-aligned bounding box of the ROI.

Next, we binarize the small portion of the edge image $\mathcal{B}$. Subsequently, we use k-means, $k = 2$, to divide and group each portion vertically of the binary image with a sliding window Δ, and discriminate the wave arms. In our experiments, we set Δ to 5 pixels. According to our experience, the results of the curve fitting process that follows do not differ when choosing Δ between 3 and 9 pixels. We choose the wave-arm closest to the camera, because is the least affected by the turbulence inside the wake. In addition, its troughs are less affected by errors when we perform the rectification of the ROI. The objective of the ROI rectification is to eliminate from the image of the mean water plane the projective distortion introduced by the camera, simulating an aerial view of the ROI. For that, we use the line at infinity $\mathbf{l}_\infty$ of the water plane to remove affine distortion, and the camera height h above sea level to eliminate projective ambiguity.

After rectifying the ROI image of the chosen wave arm, the discrete set of points obtained in may be corrupted by noise, which makes it challenging to find the troughs of the wave. We use the LOcally WEighted Scatter-plot Smoother (LOWESS) algorithm [9] to smooth the digital curve.

One finds a set of crests or a set of troughs as the curve maximum or minimum, depending on the direction of the vessel with respect to the camera. Since we have the curve that corresponds to the arm closest in the V-shaped pattern, we can find the crests and troughs as follows:

- When the vessel goes to the right in the input image $\mathcal{I}$, the curve maximum and minimum correspond, respectively, to the wave arm's troughs and crests;
- When the vessel goes to the left in the input image $\mathcal{I}$, the curve maximum and minimum correspond to the wave arm crests and troughs.

We avoid the identification of noisy troughs (or crests) by imposing a minimum horizontal distance of $\psi = 20$ meters between valid consecutive troughs (or crests), and by extracting only the two minimums/maximums (depending on the case). The value of ψ was empirically defined based on the observation that with a wavelength of approximately 20 meters, the speed is close to 10 knots and, most vessels that leave visible tracks move at higher speeds.

D. Vessel speed estimation

To solve the inverse Kelvin wake problem, we need to calculate the Euclidean distance in the world coordinate system between at least two consecutive troughs or crests. The two consecutive troughs or crests are found in Section III-C.

Once the two wave troughs (or crests) are found, the vessel speed can be estimated using the wavelength of the transverse components of the Kelvin wake structure (Fig 2). The wavelength can be estimated using the distance between successive troughs (or crests), and from the wavelength one can estimate vessel's speed [4]. We compute the wavelength λ by replacing D in $\lambda = \frac{\sqrt{3}}{2}D$, where D is the Euclidean distance (in meters) between the location of troughs (or crests).

Finally, the speed (in knots) of the vessel is:

$$U = 1.944\sqrt{\frac{g}{2\pi}\lambda}, \tag{4}$$

where $g \approx 9.80665\ m/s^2$ is the acceleration of gravity. Since $knot$ is the unit of measurement of speed used for maritime navigation, one has to multiply by 1.944 to convert from meters per second to $knots$.

IV. Experiments and Results

In the experiments, images of moving vessels were acquired under natural lighting and different weather conditions. A total of 40 images was obtained, where 23 of them were used to analyze the results (Figure 4 shows some samples).

(a) Unfavorable weather condition

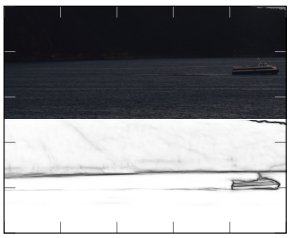

(b) Low natural lighting

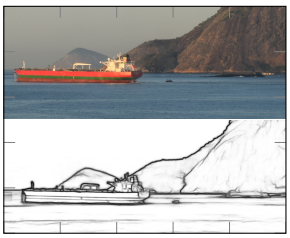

(c) An slow merchant ship

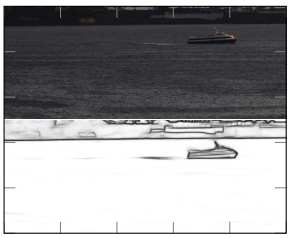

(d) Low natural lighting

Fig. 3. Cropped version of some images were our approach could not detect wave arms having at least two well defined troughs in the edge image.

The remaining 17 out of the original 40 images were not considered because they were taken under unfavorable weather conditions (Fig. 3 (a)) and low natural lighting (Fig. 3 (b) and (d)) that prevented our approach from being successful on detecting the troughs. Besides, some vessels on those images were merchant ships (Fig. 3 (c)). As such, their speed must be low because they were close to a port area. In all those cases, the traces left by the vessels or at least two troughs cannot be distinguished even by human observers. The procedures described in Section III were implemented in Python 2.

The images were taken using a Nikon D3300 camera with 24.2 megapixels and encoded in JPG format file. The lens model used was an AF-S DX NIKKOR, with $18 \sim 55\ mm$ focal length. The captured images' resolution is 6000×4000 pixels. The ROI size lying on plane $\mathbf{\Pi}$ was intentionally set to $W_{ROI} \times H_{ROI} = 180 \times 90$ meters to cover the wave arms. The camera was mounted in two places. The camera height was $h = 27.79$ and $h = 23.88$ meters approximately. A radar designed to monitor vessels was used as a resource to validate the proposed method. The radar is a FAR $-$ 21 $\times$ 7 series of X and S-band, with a 19-inch LCD screen. The radar screen includes the name and $knot$ speed of the tracked vessel.

Table I shows the identification of the vessel (column Model), the weather condition at which the pictures were taken (column Weather) and the speed measured by the radar (column U). Of the 23 images used, 22 are of two different passenger vessels (models HSC and MC25) and one is a tugboat (image i7, Fig. 4 (d)).

Considering that the data used as input (e.g., the y-coordinate of the endpoints of the vanishing line, camera height, the reference corner of the ROI and direction of the vessel in image space) are subject to errors, it is expected that the estimated speeds also have uncertainty. By comparing the computed values and the speeds measured by the radar, it is possible to have an idea of the developed technique's accuracy and precision. In Section IV-A, we analyze the relative error of our estimations. Sections IV-B and IV-C present the analysis of confidence intervals computed using sampling and first-order error propagation.

TABLE I

INFORMATION PER CAPTURED IMAGE, WHERE U DENOTES THE SPEED MEASURED BY A RADAR (GROUND TRUTH), $\hat{U}$ IS THE SPEED ESTIMATED BY OUR APPROACH USING THE WAVE ARMS TROUGHS, AND ε_a AND ε_r ARE, RESPECTIVELY, THE ABSOLUTE AND RELATIVE ERRORS OF ESTIMATIONS.

Image	Vessel Model	Weather	Speed ($knots$)		Error	
			U	$\hat{U}$	ε_a	ε_r
i1	HSC	Cloudy	18.2	18.339	0.139	0.008
i2	$MC25$	Cloudy	20.6	21.533	0.933	0.045
i3	$MC25$	Cloudy	20.5	20.609	0.109	0.005
i4	$MC25$	Cloudy	19.2	19.434	0.234	0.012
i5	$MC25$	Cloudy	17.3	16.683	0.617	0.036
i6	$MC25$	Cloudy	17.1	16.530	0.570	0.033
i7	$Other$	Cloudy	9.2	19.262	10.062	1.094
i8	$MC25$	Cloudy	19.5	19.288	0.212	0.011
i9	HSC	Cloudy	15.6	15.984	0.384	0.025
i10	HSC	Cloudy	16.5	16.611	0.111	0.007
i11	$MC25$	Cloudy	20.4	20.771	0.371	0.018
i12	$MC25$	Cloudy	20.4	20.543	0.143	0.007
i13	$MC25$	Cloudy	17.3	16.846	0.454	0.026
i14	$MC25$	Cloudy	19.6	20.533	0.933	0.048
i15	$MC25$	Cloudy	19.1	19.861	0.761	0.040
i16	$MC25$	Cloudy	20.2	22.120	1.920	0.095
i17	$MC25$	Cloudy	20.3	20.638	0.338	0.017
i18	$MC25$	Scattered storm	18.9	19.617	0.717	0.038
i19	$MC25$	Partly cloudy	17.5	17.342	0.158	0.009
i20	$MC25$	Partly cloudy	17.6	17.808	0.208	0.012
i21	$MC25$	Partly cloudy	17.8	18.947	1.147	0.064
i22	$MC25$	Partly cloudy	20.3	16.490	3.810	0.188
i23	$MC25$	Partly cloudy	16.8	16.084	0.716	0.043

A. Analysis of relative error

Relative error $\varepsilon_r = \varepsilon_a / U$ indicates the proportion of the absolute error $\varepsilon_a = |\hat{U} - U|$ of an estimated value $\hat{U}$ concerning the true value U. We have used ε_r to determine the accuracy of our approach. In Table I, the absolute error is given in $knots$. $\hat{U}$ is calculated by applying the proposed method, while U is the measurement made by the radar.

We use the troughs of the closest wave arms to estimate the $\hat{U}$ values presented in Table I. Those troughs are the least affected by the noise introduced by the vessel's turbulence and the distortion of rectified elements that are not in the actual mean water plane. According to Table I, relative errors are below 2% for ten images, in the $[2\%, 4\%]$ interval in six cases, in the $(4\%, 5\%]$ range in three images, and between 5% and 10% in three cases. Only image i7 (Fig. 4 (d)) had a relative error that surpassed the true measure (109%). The explanation for this behavior is that the trace left by the tugboat was weak because it was at 9.2 $knots$ speed, and we have set the ψ parameter for the minimum horizontal distance between valid consecutive trough to 20 meters, limiting estimated speeds to a minimum of 10 $knots$. The mean and median relative errors in Table I are, respectively, 8.18% and 2.60%. The mean relative error was clearly affected by the result in image i7. Observing

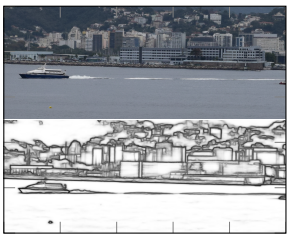

(a) Image i1, $U = 18.2\ knots$, $\hat{U} = 18.34\ knots$

(b) Image i2, $U = 20.6\ knots$, $\hat{U} = 21.53\ knots$

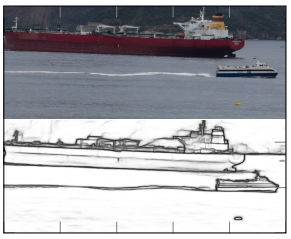

(c) Image i5, $U = 17.3\ knots$, $\hat{U} = 16.68\ knots$

(d) Image i7, $U = 9.2\ knots$, $\hat{U} = 19.26\ knots$

(e) Image i13, $U = 17.3\ knots$, $\hat{U} = 16.85\ knots$

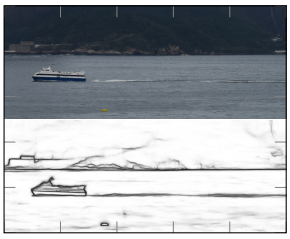

(f) Image i16, $U = 20.2\ knots$, $\hat{U} = 22.12\ knots$

(g) Image i18, $U = 18.9\ knots$, $\hat{U} = 19.62\ knots$

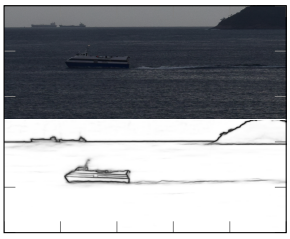

(h) Image i22, $U = 20.3\ knots$, $\hat{U} = 16.49\ knots$

Fig. 4. Cropped version of some images used in the experiments. Image i1 shows HSC passenger vessels. Images i2, i5, i13, i16, i18, and i22 show MC25 passenger vessels. Image i7 shows another vessel model. Where U denotes the speed measured by a radar (ground truth), $\hat{U}$ is the speed estimated by our approach using the wave arms troughs

the robust statistics provided by the median, we conclude that the proposed method is accurate.

B. Analysis of confidence intervals estimated from samples

In practice, each image presented in Table I provides one sample on which we can estimate speed. One way to assess the accuracy of the technique is by analyzing the variation in speed estimates obtained for the same vessel considering as input a set of images captured under similar conditions. Unfortunately, we couldn't capture enough images of each vessel at the same time to produce confidence intervals to analyze the accuracy of our approach. To simulate several image captures of the same ship, we have introduced small variations in the input variables that are considered sources of uncertainty in each captured image. We produce $n = 100$ Gaussian-distributed variations of the original set of input values of each image in Table I, generating samples from which we compute speeds and their confidence intervals:

$$CI(\gamma) = \left[\bar{U} - t_\gamma \frac{s_U}{\sqrt{n}}, \bar{U} + t_\gamma \frac{s_U}{\sqrt{n}}\right], \tag{5}$$

where $\bar{U}$ is the sample mean speed, s_U is the sample standard deviation, t_γ is a t-Student variable with $n-1$ degrees of freedom, and γ is the confidence level.

Fig. 5 (top) shows the confidence intervals with $\gamma = 99.8\%$ calculated for the vessels using sampling (Table I). For most of them, mean speed $\bar{U}$ is close to the true speed U, which is included in the respective confidence interval. For some cases where the true speed is outside the confidence interval (images i6, i11, i14, and i21) the distance to interval's limits is negligible, ranging from 0.05 to $0.50\ knots$. The narrowest confidence intervals are for images i10 and i3, respectively, with 0.30 and $0.50\ knots$ wide. The cases with most considerable distances between U and $\bar{U}$ and whose confidence interval does not include the true speed are images i7, i16, and i22. The problem with image i7 was discussed in Section IV-A. For image i16, the location of the troughs was affected by weather conditions. For image i22, low natural lighting made the trail of the vessel very blurred.

Including all cases presented in Fig. 5 (top), the largest confidence intervals are 2.86 and $1.78\ knots$ for images i16 (Fig. 4 (f)) and i22 (Fig. 4 (h)), respectively. The median size is only $0.3\ knots$. The variations of values reported by the radar for three consecutive speed measurements for vessels images i19 to i21, images i4 to i6 and images i11 to i13 are, respectively, 0.3, 2.1 and $3.1\ knots$. Thus, we concluded that the proposed approach is accurate. But we cannot make a strong statement in this regard because each interval was calculated using samples generated from one image.

C. Analysis of confidence intervals estimated using error propagation

We analyze the confidence intervals produced by the first-order error propagation approach and compare them to the intervals produces by sampling.

First-order error propagation may give the correct Gaussian uncertainty for the resulting estimations whether the uncertainty on input variables follows Gaussian distributions and the process for computing the resulting values is linear. Otherwise, it provides the first-order approximation of the error [10].

To verify which is the case of our approach, we have used the Shapiro-Wilk [11] test to check whether the resulting samples produced in Section IV-B fits Gaussian distributions. Images i7, i16, i19, i22, and i23 did not pass the test.

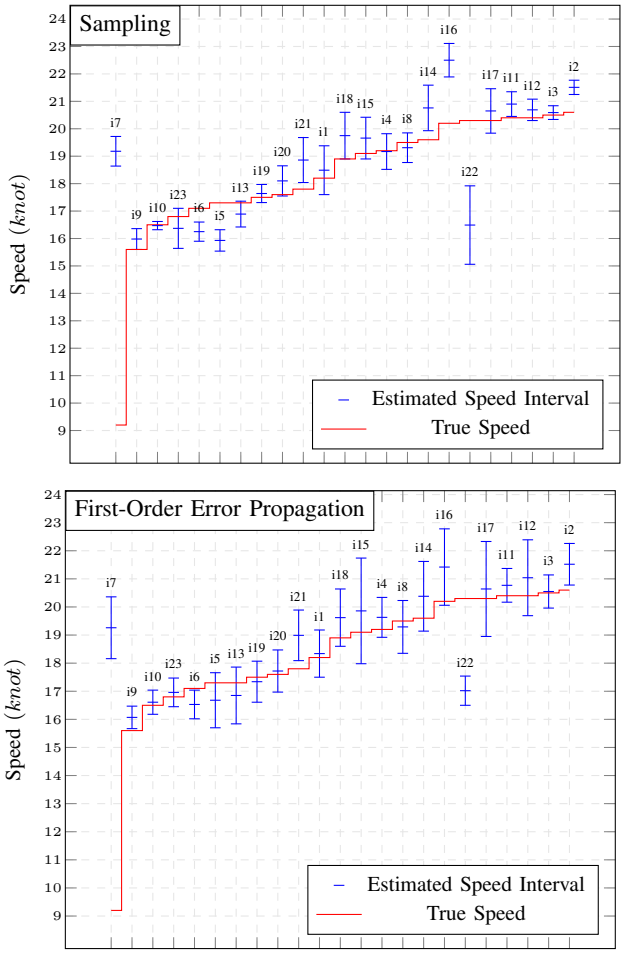

Fig. 5. Confidence intervals ($\gamma = 99.8\%$) computed using sampling (top) and first-order error propagation (bottom). Images sorted by vessel speed.

The ratio $r = s_U/\sigma_{\hat{U}}$ between the standard deviations computed from sampling and propagation shows that the first-order error propagation approach is equivalent to and slightly more conservative than the sampling-based approach. The only exceptions were $r > 1$ are images i1, i22, and i23. In 16 cases, $0.4 \leq r \leq 1$. This reflects in the result presented in Fig. 5 (bottom), where only two confidence intervals clearly do not include the true speeds (images i7 and i22), and four almost include them (images i2, i6, i9, and i21). Notice that images i7, i22, and i23 did not pass the normality test.

The narrowest intervals in Fig. 5 (bottom) have 0.80 and 0.86 $knots$ length, while the widest are for images i17, 3.38 $knots$, and i15, 3.76 knots. Using first order error propagation, the mean size of the confidence intervals was 0.942 $knots$, and the median size was 0.46 $knots$.

With the help of error propagation, it is easy to detect cases where more considerable uncertainty is included in the calculated speeds because this approach does not require several samples.

V. Conclusion

We presented a method for estimating vessel speed from single perspective projection images. The approach uses geometric constraints to remove perspective distortion from images of traces of a moving vessel, curve fitting and peak detection to identify troughs in the cusp wave arms and natural constraints on components of Kelvin wakes to compute vessel speed. Statistical methods were used in the verification of the accuracy and precision of the proposed approach and the theory of propagation of errors was used to give a notion of quality in the estimated speeds from a single observation. We believe that our algorithm can be used for maritime surveillance, using drones and smart lighthouses.

To be able to consider the use of our technique in real situations, it is necessary to draw some recommendations:

1) Lighting conditions affect edge detection and, consequently, the detection of wave arms. In our experiments, we had no problems in daylight, but it was not always possible to process images captured at dawn or dusk, and, indeed, our solution cannot be applied at night. The same applies to rain and fog.
2) Due to geographical restrictions in our experiments, we used images of the vessel port and starboard, going to the left and right direction of the camera, moving at a linear course, and (supposedly) constant speed. However, we believe that our approach is robust to variations in camera orientation since it is possible to see the troughs at the wake envelope, even at grazing angles.
3) As demonstrated in our experiments, well-defined capillary wakes due to wind and, possibly, generated by nearby vessels may affect the Kelvin wake structure. However, we believe that this is a problem that can be overcome by detecting wakes crossing.
4) Since the method is applied to a single image, the use of video could provide dozens of independent measurements per second, which could be combined to reduce error or eliminate spurious estimates.
5) Although we did not try in our experiments, preprocessing the image to, for example, increase contrast, could help in the detection of traces.

The complete work is described in [12], and it has led to two articles so far:

- The first presented at the 2019 IEEE International Conference on Image Processing (Qualis A1) [13]; and
- The second is under review in the Patterns Recognition journal (Qualis A1) [14].

Acknowledgment

This work was partially supported by CNPq (311.037/2017-8) and FAPERJ (E-26/202.718/2018) agencies. J. L. Huillca was sponsored by a CAPES fellowship. The authors thank Arthur Ayres Neto (LAGEMAR-UFF), Fabio Hochleitner (LAMCE-COPPE-UFRJ), Artur Brandão, and Jacó Julio de Souza Costa for assistance in building the dataset.

REFERENCES

[1] L. Tetley and D. Calcutt, *Electronic Navigation Systems*, 3rd ed. Butterworth-Heinemann, 2001.

[2] W. Thomson, "On ship waves," *Proc. Inst. Mech. Eng.*, vol. 38, pp. 641–649, 1887.

[3] N. Wawrzyniak, T. Hyla, and A. Popik, "Vessel detection and tracking method based on video surveillance," *Sensors*, vol. 19, p. 5230, 2019.

[4] A. Panico, M. D. Graziano, and A. Renga, "SAR-based vessel velocity estimation from partially imaged Kelvin Pattern," *IEEE Geosci. Remote. Sens. Lett.*, vol. 14, no. 11, pp. 2067–2071, 2017.

[5] A. Broggi, P. Cerri, P. Grisleri, and M. Paterlini, "Boat speed monitoring using artificial vision," in *Proc. ICIAP*, P. Foggia, C. Sansone, and M. Vento, Eds. Springer Berlin Heidelberg, 2009, pp. 327–336.

[6] S. Workman, M. Zhai, and N. Jacobs, "Horizon lines in the wild," in *Proc. BMVC*, 2016, pp. 20.1–20.12.

[7] R. Hartley and A. Zisserman, *Multiple View Geometry in Computer Vision*. Cambridge University Press, 2004.

[8] Y. Liu, M. M. Cheng, X. Hu, J. Bian, L. Zhang, X. Bai, and J. Tang, "Richer convolutional features for edge detection," *IEEE Trans. Pattern Anal. Mach. Intell.*, vol. 41, no. 8, pp. 1939–1946, 2019.

[9] R. Wilcox, "The regression smoother LOWESS: A confidence band that allows heteroscedasticity and has some specified simultaneous probability coverage," *J. Mod. Appl. Stat. Methods*, vol. 16, pp. 29–38, 2017.

[10] L. G. Parratt, *Probability and experimental errors in science : an elementary survey*. John Wiley & Sons, Inc., 1961.

[11] S. S. Shapiro and M. B. Wilk, "An analysis of variance test for normality (complete samples)," *Biometrika*, vol. 52, no. 3-4, pp. 591–611, 1965.

[12] J. L. Huillca, *Computing vessel velocity from single perspective projection images*. Master's thesis, UFF, Rio de Janeiro, Brasil, 2020.

[13] J. L. Huillca and L. A. F. Fernandes, "Computing vessel velocity from single perspective projection images," in *Proc. ICIP*, 2019, pp. 325–329.

[14] J. L. Huillca and L. A. Fernandes, "Using error propagation to estimate confidence intervals for the speed of vessels from single images," *Pattern Recognition*, 2021, under review.